Acta Crystallographica Section A
Foundations and Advances
ISSN 2053-2733

Received 5 February 2014
Accepted 26 June 2014

An algorithm for calculating diffraction profiles of 2θ scans for multiple diffraction from crystals and thin films

Hsin-Yi Chen,[a] Mau-Sen Chiu,[b] Chia-Hung Chu[b] and Shih-Lin Chang[a,b]*

[a]Department of Physics, National Tsing Hua University, Hsinchu, Taiwan, and [b]National Synchrotron Radiation Research Center, Hsinchu, Taiwan. Correspondence e-mail: slchang@nsrrc.org.tw

An algorithm is developed based on the dynamical theory of X-ray diffraction for calculating the profiles of the diffracted beam, *i.e.* the diagrams of the intensity distribution *versus* 2θ when a crystal is fixed at an angle of its maximum diffracted intensity. Similar to Fraunhofer (far-field) diffraction for a single-slit case, in the proposed algorithm the diffracted beam from one atomic layer excited by X-rays is described by the composition of $(N + 1)$ coherent point oscillators in the crystal. The amplitude and the initial phase of the electric field for each oscillator can be calculated based on the dynamical theory with given boundary conditions. This algorithm not only gives diffraction profiles but also provides the contribution of the excitation of modes when extremely asymmetric diffraction is involved in the diffraction process. Examples such as extremely asymmetric two-beam surface diffraction and three-beam surface diffraction are presented and discussed in detail.

1. Introduction

The dynamical theory has the capability to cope with the interaction of X-rays with matter during diffraction occurrence in large, perfect crystalline systems. In 1997, Stetsko and Chang introduced an algorithm using a Cartesian coordinate system and showed that the fundamental equations of the wavefield can be converted into an eigenvalue equation by algebraic linearization without further assumption and approximations for X-ray polarization (Stetsko & Chang, 1997). The algorithm developed by Stetsko & Chang (1997) is quite general and is not limited to extremely asymmetric diffraction geometries or back diffraction. It is also suitable for wide-angle diffraction geometries. Based on this algorithm and the dynamical theory of X-ray diffraction, the diagram of intensity distribution *versus* the θ scan (rocking curve), φ scan (Renninger scan) and energy scan can be calculated.

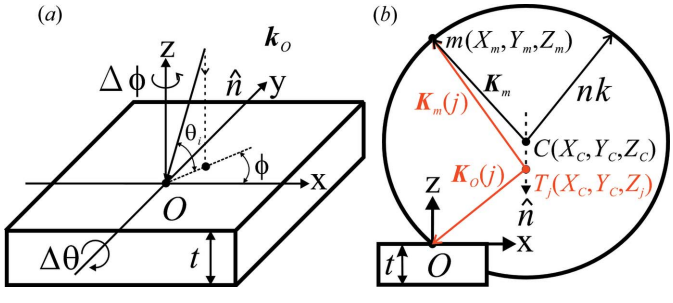

Figure 1
(*a*) The Cartesian coordinate frame. $\hat{\boldsymbol{n}}$ is inward surface normal and t is the thickness of the crystal. $\mathbf{k}_O$ is the incident beam, θ_i is the angle between $\mathbf{k}_O$ and the xy plane. φ is the angle between the x axis and the projection of the incident beam on the xy plane. (*b*) The geometry of the N-beam diffraction in reciprocal space (see the text for explanation).

Regarding the θ scan, the crystal is rotated along the y axis (see Fig. 1*a*) and the angular position of the detector is stationary at a given $2\theta_B$, where θ_B is the Bragg angle. This so-called rocking curve provides structural information about the crystal. For example, the width of a rocking curve determines the mosaic spread of the crystal. As for the φ scan, the crystal is rotated along the z axis (see Fig. 1*a*) along a given reciprocal-lattice vector to generate multiple-beam diffraction. In the case of the 2θ scan, however, the crystal is fixed at the incident angle θ_i at which the diffracted intensity (rocking curve) is maximum and the detector is rotated around the 2θ axis (Chang, 2004).

For an N-beam diffraction, one incident beam and $(N - 1)$ diffracted beams are involved. For surface diffraction geometry, however, surface specular reflection needs to be considered. For an extremely asymmetric diffraction such as grazing-incident and grazing-emergence diffraction, the diagram of the intensity distribution *versus* the 2θ scan would be very helpful to understand and forecast experimental data. However, the diagram of the intensity distribution *versus* the 2θ scan was not covered by that algorithm. Additional development is needed.

In this paper, we propose a new algorithm, based on the dynamical theory of X-ray diffraction, to calculate the profiles of the diffracted beams as a function of the 2θ angle (2θ scan).

We use an extremely asymmetric two-beam surface diffraction from an Si substrate and a three-beam Bragg surface diffraction from a Ge substrate as examples to illustrate the relation between the diffraction profiles and individual modes of excitation. We successfully demonstrate not only the 2θ diffraction profiles but also the connection between the diffraction profiles and the excitation of modes for asymmetric diffraction situations. This algorithm can also determine whether the diffracted beam is of single-mode or multi-mode nature (Chen *et al.*, 2014).

2. Theoretical considerations

Darwin and Ewald initially developed the dynamical theory of X-ray diffraction in order to explain the primary extinction (Darwin, 1914; Ewald, 1916). Max von Laue introduced the dielectric constant in crystalline materials as a complex periodic function of space, and the X-ray wavefunctions are interpreted as Bloch waves (von Laue, 1931). The dynamical theory of X-ray diffraction has been devised not only for plane-wave X-rays but also for spherical-wave X-rays (Kato, 1960; Kohn *et al.*, 2000). A spherical wave of X-ray diffraction can account for X-ray imaging (Kohn *et al.*, 2013). Here, the incident beam waves are assumed to be plane-wave X-rays. Then the interaction of X-rays with the crystal can be described by the fundamental equation of the wavefield.

For N-beam diffraction, all N reciprocal-lattice points are on the surface of the Ewald sphere. The fundamental equation of the wavefield can be written as equation (1) (Stetsko & Chang, 1997; Authier, 2005; Chang, 2004):

$$(\mathbf{K}_m \cdot \mathbf{K}_m - k^2)\mathbf{E}_m = (\mathbf{K}_m \cdot \mathbf{E}_m)\mathbf{K}_m + k^2 \sum_{n=0}^{N-1} \chi_{m-n}\mathbf{E}_n, \quad (1)$$

where $m = 0, 1, 2, \cdots, N-1$. k is the inverse of the wavelength λ of the incident beam ($k = 1/\lambda$). χ_{m-n} is the dielectric susceptibility of the crystal for the $(m-n)$ reflection. $\mathbf{K}_m$ is the wavevector of the mth reflection inside the crystal and $\mathbf{E}_m$ is the corresponding electric field. Information on the

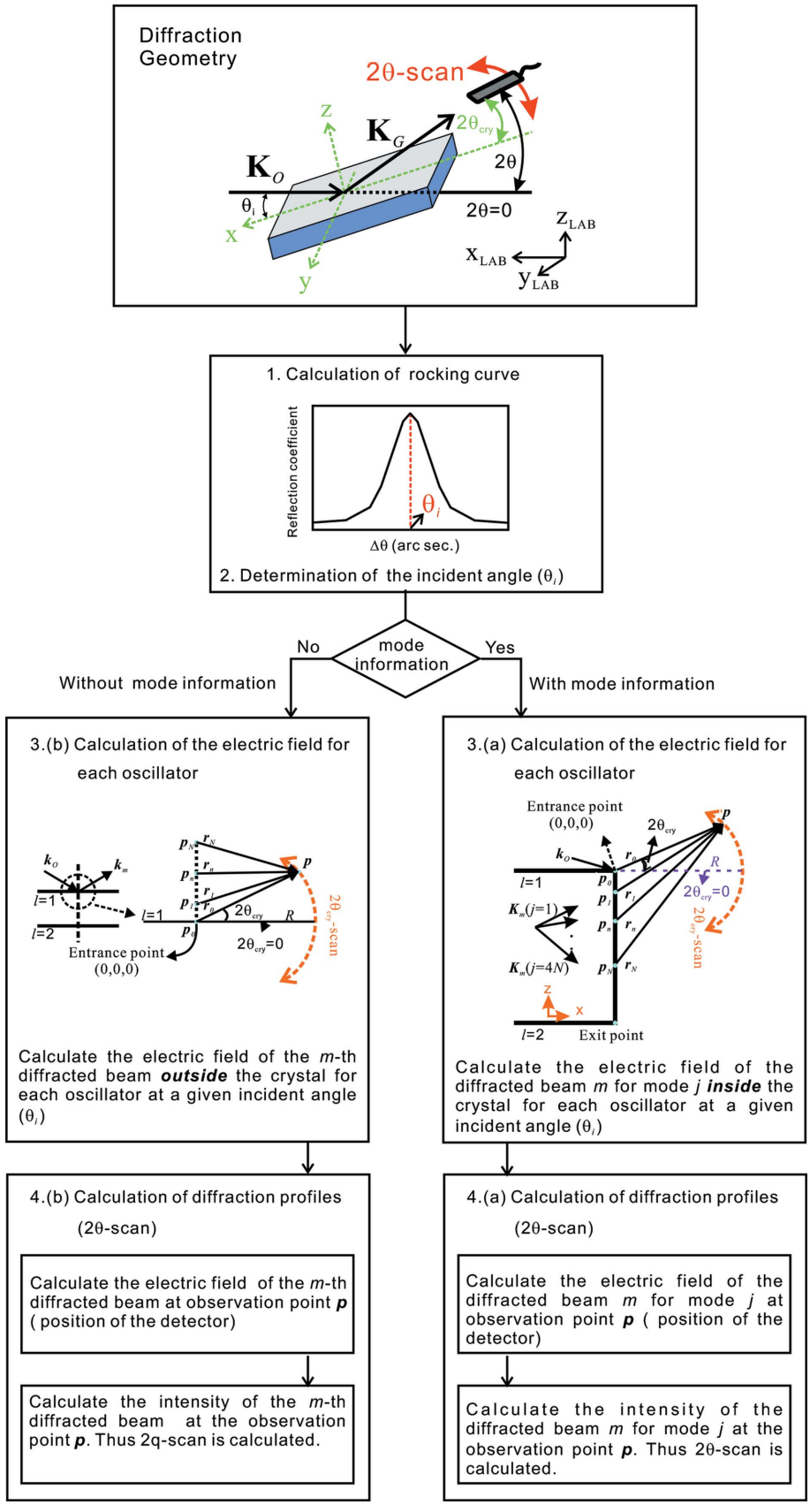

Figure 2
The calculation procedures for diffraction profiles (2θ scan).

electromagnetic waves inside and outside the crystal can be determined by the boundary conditions.

Stetsko & Chang (1997) proposed an algorithm which deals with an N-beam diffraction situation in a single crystal. This algorithm without assumption or approximation is highly favourable for calculation in any kind of diffraction geometry, including both symmetric and asymmetric cases, such as Laue transmission, Bragg reflection, back diffraction, grazing-incidence diffraction and grazing-emergence diffraction. In the algorithm, the fundamental equation of the wavefield, equation (1), is decomposed into scalar equations *via* a Cartesian coordinate representation (Stetsko & Chang, 1997). Furthermore, the fundamental equation of the wavefield can be simplified as an eigenvalue equation in $4N \times 4N$ matrices.

The $4N$ eigenvalues and eigenvectors can be determined by solving the eigenvalue equation. An eigenvalue is denoted as z_j with $j = 1, \cdots, 4N$, respectively. The real part of the eigenvalue z_j represents the z component of the jth tie point on the dispersion surface. The coordinate of the jth tie point and the centre of the Ewald sphere can be expressed as $T_j(X_C, Y_C, z_j)$ and $C(X_C, Y_C, Z_C)$ as shown in Fig. 1(*b*). The imaginary part of the eigenvalue z_j is proportional to the linear absorption coefficient. In this Cartesian coordinate frame (see Fig. 1*a*), the z axis is defined to be perpendicular to the entrance crystal surface and outward, and both x and y axes are parallel to the entrance crystal surface. In Fig. 1(*b*), the geometry of the N-beam diffraction is shown in reciprocal space. The wavevectors of diffracted beams inside the crystal are drawn from the tie points on the dispersion surface to the reciprocal-lattice points. **k** and **K** are wavevectors outside and inside the crystal, respectively. The radius of the Ewald sphere is nk, where n is the index of refraction. The reciprocal-lattice points are expressed as (X_m, Y_m, Z_m) and the origin of the reciprocal-lattice vector is $O(0, 0, 0)$. **Om** is the reciprocal-lattice vector of a given reflection m. Referring to vector algebra, the wavevector of the diffracted beam propagating inside the crystal can be written as

$$\mathbf{K}_m(j) = (X_m - X_C, Y_m - Y_C, Z_m - z_j) = (x_m, y_m, z_{mj}), \quad (2)$$

where $X_C = (1/\lambda)\cos\theta_i \cos\varphi$, $Y_C = (1/\lambda)\cos\theta_i \sin\varphi$ and $z_{mj} = Z_m - z_j$. Moreover, the eigenvectors represent the electric field ratios inside the crystal with a proportionality constant c_j. The electric field of the mth diffracted beam inside the crystal, $\mathbf{E}_m$, can be written as

$$\mathbf{E}_m = \begin{pmatrix} E_m^X \\ E_m^Y \\ E_m^Z \end{pmatrix} = \sum_{j=1}^{4N} \begin{bmatrix} E_m^X(j) \\ E_m^Y(j) \\ E_m^Z(j) \end{bmatrix} = \sum_{j=1}^{4N} c_j \times \begin{bmatrix} E_m^x(j) \\ E_m^y(j) \\ E_m^z(j) \end{bmatrix} \times \psi_{jl}, \quad (3)$$

$\psi_{jl} = \exp[-2i\pi \mathbf{K}_m(j) \cdot \mathbf{r}]$ is the phase term of the mth diffracted beam at point **r** inside the crystal for the jth mode, and **r** is a position vector. At the entrance point $\mathbf{r} = (0, 0, 0)$, $l = 1$ and $\psi_{j1} = 1$, and at the exit point $\mathbf{r} = (0, 0, -t)$, $l = 2$ and $\psi_{j2} = \exp(2i\pi z_{mj} t)$.

The electric field of the mth diffracted beam outside the crystal can be written as

$$\mathbf{E}_{ml} = \begin{pmatrix} E_{ml}^x \\ E_{ml}^y \\ E_{ml}^z \end{pmatrix} \varphi_{ml} + \begin{bmatrix} E_{(e)}^x \\ E_{(e)}^y \\ E_{(e)}^z \end{bmatrix} \delta_{m0}^{l1}. \quad (4)$$

The electric field of the incident beam is $\mathbf{E}_{(e)} = [E_{(e)}^x, E_{(e)}^y, E_{(e)}^z]$, δ_{m0}^{l1} is the Kronecker delta. When $m = 0$ and $l = 1$, δ_{m0}^{l1} is 1. Otherwise, δ_{m0}^{l1} is 0. The electric field of the mth diffracted beam outside the crystal is $(E_{ml}^x, E_{ml}^y, E_{ml}^z) \times \varphi_{ml}$. The phase term of the mth diffracted beam outside the crystal is defined as $\varphi_{ml} = \exp\{-2i\pi[x_m X + y_m Y + (-1)^l K_m^z Z]\}$. Therefore, the phases at the entrance and exit surface are $\varphi_{m1} = 1$ and $\varphi_{m2} = \exp(2i\pi K_m^z t)$, respectively, where $K_m^z = -[k^2 - (x_m^2 + y_m^2)]^{1/2}$. The proportional coefficient c_j can be solved from the boundary conditions described below.

The boundary conditions for the wavefield amplitude matching at the entrance ($l = 1$) and exit ($l = 2$) crystal surfaces are both tangential components of **E** and **H**, continuous at the boundaries, as well as both normal components of **D** and **B**, continuous at the boundaries. Besides, for non-magnetic materials ($\mathbf{B} = \mu\mathbf{H} = \mathbf{H}$), the relationships among **E**, **B**, **D** and **H** are $\mathbf{D}_m = \varepsilon_0(\mathbf{E}_m + \sum_{n=0}^{N-1} \chi_{m-n}\mathbf{E}_n)$ and $\mathbf{H}_m = (\mathbf{K}_m \times \mathbf{E}_m)/k$. For an N-beam diffraction, the N diffracted beams follow the boundary conditions for both surfaces, *i.e.*

$$E_x\colon \sum_{j=1}^{4N} c_j E_m^x(j) = E_{(e)}^x \delta_{mO}^{l1} + E_{m1}^x \varphi_{ml} \quad (5)$$

$$E_y\colon \sum_{j=1}^{4N} c_j E_m^y(j) = E_{(e)}^y \delta_{mO}^{l1} + E_{m1}^y \varphi_{ml} \quad (6)$$

$$D_z\colon \sum_{j=1}^{4N} c_j \left[E_m^z(j) + \sum_{n=0}^{N-1} \chi_{m-n} E_n^z(j) \right] = E_{(e)}^z \delta_{mO}^{l1} + E_{m1}^z \varphi_{ml} \quad (7)$$

$$H_x\colon \sum_{j=1}^{4N} c_j [z_{mj} E_m^y(j) - y_m E_m^z(j)] \psi_{jl} = [K_m^z E_{(e)}^y - y_m E_{(e)}^z] \delta_{mO}^{l1} + [(-1)^l k_m^z E_{m1}^y - y_m E_{m1}^z] \varphi_{ml} \quad (8)$$

$$H_y\colon \sum_{j=1}^{4N} c_j [x_m E_m^z(j) - z_{mj} E_m^x(j)] \psi_{jl} = [x_m E_{(e)}^z - K_m^z E_{(e)}^x] \delta_{mO}^{l1} + [x_m E_{ml}^z - (-1)^l k_m^z E_{m1}^x] \varphi_{ml} \quad (9)$$

$$B_z\colon \sum_{j=1}^{4N} c_j [y_m E_m^x(j) - x_m E_m^y(j)] \psi_{jl} = [y_m E_{(e)}^x - x_m E_{(e)}^y] \delta_{mO}^{l1} + (y_m E_{ml}^x - x_m E_{m1}^y) \varphi_{ml}. \quad (10)$$

The unknown c_j can be determined by merging equations (5)–(10) using a linear combination and eliminating electric fields E_{ml}^x, E_{ml}^y and E_{ml}^z. The derived process can be found in Stetsko & Chang (1997). The details of programming procedures for dynamical calculation can be found in Chiu *et al.* (2008).

3. An algorithm for calculating the diffraction profile of a 2θ scan

The algorithm for X-ray crystal diffraction patterns (2θ scan) is similar to that for Fraunhofer diffraction. According to Fraunhofer (far-field) diffraction for a single-slit case, the slit could be depicted as a linear array of $(N + 1)$ coherent iden-

tical point oscillators. The diffraction pattern in space can be calculated from the electrical field of each oscillator (Hecht, 2002; Saleh & Teich, 2007). In the proposed algorithm for calculating the X-ray crystal diffraction profile, the 2θ scan, the diffracted beam from one atomic layer excited by X-rays can also be described by the composition of $(N+1)$ coherent point oscillators. The amplitude and initial phase of the electric field for each oscillator are calculated based on the dynamical theory of X-ray diffraction with given boundary conditions. The $(N+1)$ oscillators are either near the entrance surface ($l=1$) or the exit surface ($l=2$) depending on whether the diffraction geometry is Bragg or Laue. For a Bragg case, the Bragg diffracted beam is reflected from the crystal and leaves the entrance surface, while for a Laue case, the diffracted beam transmits through the crystal and leaves the crystal from the exit surface. The atomic layer excited by X-rays contributes considerably to the diffracted beam. Its depth is related to the extinction distance for the reflection geometry and *Pendellösung* distance for the transmission geometry. It can be expressed as $L=\lambda(\gamma_O\gamma_G)^{1/2}/|\chi_G|$, where λ is wavelength, χ_G is the electric susceptibility of the G-beam reflection, and γ_O and γ_G are the direction cosines of the incident and diffracted beams with respect to the inward surface normal $\hat{\boldsymbol{n}}$ (Authier, 2005; Als-Nielsen & McMorrow, 2011). The crystal thickness is t. Moreover, this algorithm can be divided into two schemes. For the first scheme, the diffraction pattern of the 2θ scan is calculated by using the electric fields inside the crystal for each oscillator, and the connection between the diffraction profile and the excitation of mode can be seen from the calculated results. Usually for wide-angle diffraction, the correlation between the measured intensities and modes cannot be distinguished, unless the diffraction is extremely asymmetric. For the second scheme, the electric fields outside the crystal are adopted, and the calculated result shows only the diffraction pattern without mode information. This is due to the fact that the electric fields outside the crystal for each oscillator given by equation (4) have a contribution from all the possibly excited modes. It is therefore impossible to tell which electric field outside the crystal resulted from which individual modes. In fact, both schemes give the same diffraction profiles, intensity distribution and peak position. Fig. 2 shows the concept of the calculation procedures for diffraction profiles (2θ scan). The main steps are:

(1) Calculation of the rocking curve based on the X-ray dynamical theory (Stetsko & Chang, 1997; Chiu *et al.*, 2008).

(2) Determination of the incident angle ($\theta_{\rm i}$) at the peak position of the rocking curve: the diffraction profiles (2θ scan) are calculated for fixed $\theta_{\rm i}$. Usually $\theta_{\rm i}$ is the exact diffraction angle, namely the Bragg angle.

(3) Calculation of the electric field for each oscillator:

(*a*) With mode information: calculate the electric field of the diffracted beam m for mode j inside the crystal for each oscillator at a given incident angle ($\theta_{\rm i}$) by using equation (3) or equation (11).

(*b*) Without mode information: calculate the electric field of the mth diffracted beam outside the crystal for each oscillator at a given incident angle ($\theta_{\rm i}$) by using equation (4) or equation (16).

The calculations are based on the dynamical theory of X-ray diffraction with given boundary conditions.

(4) Calculation of diffraction profiles (2θ scan):

(*a*) With mode information: calculate the electric field of the diffracted beam m for mode j at observation point p (position of a detector), and then calculate the intensity of the electric field at observation point p. Thus the 2θ scan is calculated.

(*b*) Without mode information: calculate the electric field of the mth diffracted beam at observation point p (position of a detector), and then calculate the intensity of the electric field at observation point p. Thus the 2θ scan is calculated.

Step (3) is the key to obtaining the diffraction profiles and showing the connection between the diffraction profiles and the excitation of modes.

3.1. 2θ scan with mode information

For the first scheme, assume that the diffracted beams propagate from the side wall of the crystal into the air. Suppose that a linear array of the $(N+1)$ coherent point oscillators are lined up parallel to the z axis inside the crystal. Figs. 3(*a*) and 3(*b*) show the schematic representation of calculating the diffraction profile of the 2θ scan at the entrance crystal surface ($l=1$) for the Bragg diffraction case and at the exit crystal surface ($l=2$) for the Laue diffraction case, respectively. Referring to equation (3), the electric field of the nth oscillator of the diffracted beam m for mode j inside the crystal can be expressed as

$$\mathbf{E}_{mj_{-in}}(\mathbf{p}_n)=c_j\times\begin{bmatrix}E_m^x(j)\\E_m^y(j)\\E_m^z(j)\end{bmatrix}\times\exp\left[-2i\pi(\mathbf{K}_{mj}\cdot\mathbf{p}_n)\right],\qquad(11)$$

where $n=0,1,\cdots,N$. $\mathbf{p}_n$ is the vector position of the nth oscillator, expressed as $\mathbf{p}_n=-p_n\hat{\boldsymbol{k}}$. Referring to equation (2), $\mathbf{K}_{mj}$ [$\mathbf{K}_{mj}=\mathbf{K}_m(j)$] stands for the wavevector of the diffracted beam m for mode j inside the crystal. The electric field of mode j of the nth oscillator outside the crystal [$\mathbf{E}_{mj}(p_n)$] can be determined by the electric field of mode j of the nth oscillator inside the crystal [equation (11)] and the boundary conditions for the wavefield amplitude matching at the side wall of the crystal (see §2). Moreover, the electric field, $\mathbf{E}_{mj}(\mathbf{p})$, at the point of observation p, can be taken as the superposition of the electric fields radiated from the oscillators on the side wall of the crystal, *i.e.*

$$\begin{aligned}\mathbf{E}_{mj}(\mathbf{p})=&\,\mathbf{E}_{mj}(\mathbf{p}_0)\times\exp[i(\mathbf{K}_{mj}\cdot\mathbf{r}_0)]+\mathbf{E}_{mj}(\mathbf{p}_1)\times\exp[i(\mathbf{K}_{mj}\cdot\mathbf{r}_1)]\\&+\cdots+\mathbf{E}_{mj}(\mathbf{p}_n)\times\exp[i(\mathbf{K}_{mj}\cdot\mathbf{r}_n)]+\cdots\\&+\mathbf{E}_{mj}(\mathbf{p}_N)\times\exp[i(\mathbf{K}_{mj}\cdot\mathbf{r}_N)].\end{aligned}\qquad(12)$$

$\mathbf{r}_n$ is the position vector from the nth oscillator to the observation point p, *i.e.* $\mathbf{r}_n=\mathbf{p}-\mathbf{p}_n$. The observation point p is at (x_p,y_p,z_p) and the position vector is expressed as $\mathbf{p}=(x_p,y_p,z_p)-(0,0,0)=[R\cos(2\theta_{\rm cry}),0,R\sin(2\theta_{\rm cry})]$. R is the distance between a sample and a detector, and $2\theta_{\rm cry}$ is the angular deviation from the position of the crystal surface.

Assume that the oscillators can be taken as point sources and are far from the observation point p. The wavefront at p can be treated as plane-like. Therefore, it should be clear that the phase term could be expressed as $\mathbf{K}_{mj} \cdot \mathbf{r}_n = |\mathbf{K}_{mj}||\mathbf{r}_n| \cos \vartheta$, where ϑ is the angle between $\mathbf{K}_{mj}$ and $\mathbf{r}_n$. Then the wave takes the form

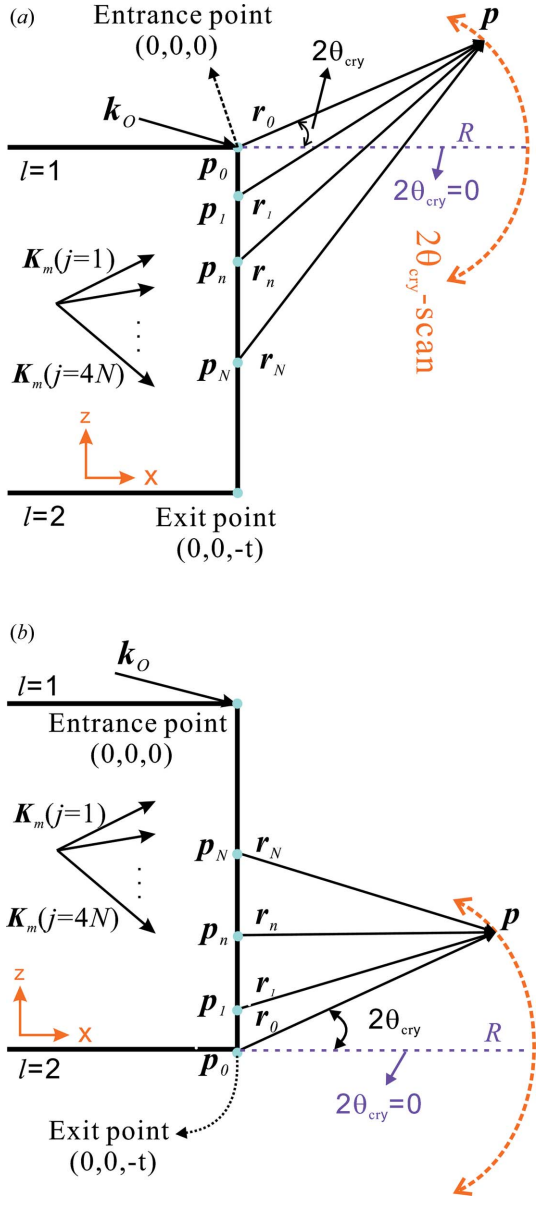

Figure 3
Schematic representation in the xz plane of the one-dimensional diffraction profile (2θ scan) algorithm with inner electric fields of the mth diffracted beam of the jth mode for (a) Bragg diffraction where $(N+1)$ oscillators are near the entrance surface, $l = 1$, and (b) Laue diffraction where $(N+1)$ oscillators are near the exit surface, $l = 2$. $\mathbf{K}_m(j)$ is the wavevector of the jth mode of the mth reflection. $2\theta_{\rm cry}$ is the angular deviation from the position of the crystal surface. The origin is at the entrance point (0, 0, 0) and the exit point is at (0, 0, $-t$). R is the distance between the origin and the observation point. The vector position of the nth oscillator and the observation point are denoted as $\mathbf{p}_n$ and p, respectively. $\mathbf{r}_n$ is the position vector from the nth oscillator to the observation point p, *i.e.* $\mathbf{r}_n = \mathbf{p} - \mathbf{p}_n$. [The observation point p is at (x_p, y_p, z_p) where $x_p = R\cos(2\theta_{\rm cry})$, $y_p = 0$, $z_p = R\sin(2\theta_{\rm cry})$.]

$$\begin{aligned}\mathbf{E}_{mj}(\mathbf{p}) = {} & \mathbf{E}_{mj}(\mathbf{p}_0) \times \exp[i(K_{mj}r_0)] + \mathbf{E}_{mj}(\mathbf{p}_1) \times \exp[i(K_{mj}r_1)] + \cdots \\ & + \mathbf{E}_{mj}(\mathbf{p}_n) \times \exp[i(K_{mj}r_n)] + \cdots \\ & + \mathbf{E}_{mj}(\mathbf{p}_N) \times \exp[i(K_{mj}r_N)]. \end{aligned} \tag{13}$$

Equation (13) is exactly the same as equation (12) because $\mathbf{K}_{mj}$ and $\mathbf{r}_n$ are along the same direction, *i.e.* $\mathbf{K}_{mj} \cdot \mathbf{r}_n = |\mathbf{K}_{mj}||\mathbf{r}_n| \cos \vartheta = |\mathbf{K}_{mj}||\mathbf{r}_n| = K_{mj}r_n$, where ϑ is 0° (Hecht, 2002).

Equation (13) can be rearranged in the form shown below:

$$\begin{aligned}\mathbf{E}_{mj}(p) = {} & \\ & \exp[i(K_{mj}r_0)] \times \big(\mathbf{E}_{mj}(\mathbf{p}_0) \times 1 + \mathbf{E}_{mj}(\mathbf{p}_1) \times \exp\{i[K_{mj}(r_1 - r_0)]\} \\ & + \cdots + \mathbf{E}_{mj}(\mathbf{p}_n) \times \exp\{i[K_{mj}(r_n - r_0)]\} + \cdots \\ & + \mathbf{E}_{mj}(\mathbf{p}_N) \times \exp\{i[K_{mj}(r_N - r_0)]\}\big), \end{aligned} \tag{14}$$

where $\mathbf{r}_n = \mathbf{p} - \mathbf{p}_n = (x_p, y_p, z_p) - (0, 0, -p_n) = [R\cos(2\theta_{\rm cry}), 0, R\sin(2\theta_{\rm cry}) - p_n]$ and $\mathbf{r}_0 = \mathbf{p} - \mathbf{p}_0 = (x_p, y_p, z_p) - (0, 0, -p_0) = [R\cos(2\theta_{\rm cry}), 0, R\sin(2\theta_{\rm cry}) - p_0]$. Thus, $|\mathbf{r}_n|$ and $|\mathbf{r}_0|$ are functions of $2\theta_{\rm cry}$. p_n is the depth of the nth oscillator from the entrance point. Notice that p_N must be smaller than the extinction length L (Authier, 2005; Als-Nielsen & McMorrow, 2011), and its scale is usually chosen as the same as the extinction L. Moreover, the number of oscillators, $(N+1)$, stands for the number of calculated data points. The scale of the quantity Δp, the distance between the adjacent oscillators $\Delta p = (p_{n+1} - p_n) = p_N/N$, is usually chosen as the same as the wavelength of the incident beam. As mentioned previously, p and $r_n - r_0$ could be expressed as a function of $2\theta_{\rm cry}$. By setting $\xi = r_n - r_0$, the electric field at p can be written as

$$\begin{aligned}\mathbf{E}_{mj}(2\theta_{\rm cry}) = {} & \\ & \exp[i(K_{mj}r_0)] \times \{\mathbf{E}_{mj}(\mathbf{p}_0) \times 1 + \mathbf{E}_{mj}(\mathbf{p}_1) \times \exp[i(K_{mj}\xi_1)] \\ & + \cdots + \mathbf{E}_{mj}(\mathbf{p}_n) \times \exp[i(K_{mj}\xi_n)] + \cdots \\ & + \mathbf{E}_{mj}(\mathbf{p}_N) \times \exp[i(K_{mj}\xi_N)]\}. \end{aligned} \tag{15}$$

The intensity of the diffracted beam at the observation point p is proportional to the square of the electric field $\mathbf{E}_{mj}(2\theta_{\rm cry})$ at p. Therefore, the intensity of a diffracted beam m for mode j at p can be expressed as $I_{mj}(2\theta_{\rm cry}) = |\mathbf{E}_{mj}(2\theta_{\rm cry}) \cdot \mathbf{E}^*_{mj}(2\theta_{\rm cry})|$. The integrated intensity I_m for a diffracted beam m is the sum of the intensities of all the modes involved, *i.e.* $I_m = \sum_{\Delta 2\theta_{\rm cry}} I_m(2\theta_{\rm cry}) \times \Delta 2\theta_{\rm cry}$, where $I_m(2\theta_{\rm cry}) = \sum_{j=1}^{4N} I_{mj}(2\theta_{\rm cry})$. Notice that the interval of each step, $\Delta 2\theta_{\rm cry}$, must be smaller than the full width at half-maximum (FWHM) of the diffracted beam in the x direction.

3.2. 2θ scan without mode information

In the second scheme, the diffraction pattern is calculated by using the electric fields *outside* the crystal. The mth diffracted beams propagating into the air from the top ($l = 1$, for the Bragg diffraction case) and the bottom ($l = 2$, for the Laue diffraction case) of the crystal are shown in Figs. 4(a) and 4(b), respectively. In Fig. 4, the symbols are the same as those used in Fig. 3. Suppose that there is a linear array of $(N+1)$ coherent point oscillators outside the crystal. $\mathbf{k}_O$ and $\mathbf{k}_m$ stand

for the wavevector of the incident beam and the wavevector of the mth diffracted beam outside the crystal, $k = |\mathbf{k}_O| = |k_m|$. $\mathbf{E}_{ml}$ is the electric field of the mth diffracted beam outside the crystal. This indicates that both $\mathbf{E}_{ml}$ and k are indistinguishable to excitation of modes. Referring to equation (4), the electric field of the nth oscillator for a diffracted beam m outside the crystal can be expressed as

$$\mathbf{E}_{ml}(\mathbf{p}_n) = \begin{pmatrix} E_m^X l \\ E_m^Y l \\ E_m^Z l \end{pmatrix} \times \varphi_{ml}, \tag{16}$$

where $n = 0, 1, \cdots, N$. The phase term of the nth oscillator for a diffracted beam m outside the crystal is defined as $\varphi_{ml} = \exp\{-2i\pi[x_m X + y_m Y + (-1)^l K_m^z Z]\} = \exp[2i\pi(-1)^l K_m^z p_n]$, where $Z = -p_n\hat{\boldsymbol{k}}$. In accordance with the principle of superposition, the electric field $\mathbf{E}_m(\mathbf{p})$ of the diffracted beam m at the point of observation p can be written as

$$\begin{aligned}\mathbf{E}_{ml}(\mathbf{p}) = {} & \mathbf{E}_{ml}(\mathbf{p}_0) \times \exp[i(kr_0)] + \mathbf{E}_{ml}(\mathbf{p}_1) \times \exp[i(kr_1)] + \cdots \\ & + \mathbf{E}_{ml}(\mathbf{p}_n) \times \exp[i(kr_n)] + \cdots + \mathbf{E}_{ml}(\mathbf{p}_N) \times \exp[i(kr_N)].\end{aligned} \tag{17}$$

Then, the electric field at p can be expressed as a function of $2\theta_{\rm cry}$ as

$$\begin{aligned}\mathbf{E}_{ml}(2\theta_{\rm cry}) = {} & \exp[i(kr_0)] \times \{\mathbf{E}_{ml}(\mathbf{p}_0) \times 1 + \mathbf{E}_{ml}(\mathbf{p}_1) \times \exp[i(k\xi_1)] \\ & + \cdots + \mathbf{E}_{ml}(\mathbf{p}_n) \times \exp[i(k\xi_n)] + \cdots \\ & + \mathbf{E}_{ml}(\mathbf{p}_N) \times \exp[i(k\xi_N)]\}.\end{aligned} \tag{18}$$

Hence, the integrated intensity I_{ml} for a diffracted beam m is expressed as

$$I_{ml} = \sum_{\Delta 2\theta_{\rm cry}} I_{ml}(2\theta_{\rm cry}) \times \Delta 2\theta_{\rm cry}, \tag{19}$$

where $I_{ml}(2\theta_{\rm cry}) = |\mathbf{E}_{ml}(2\theta_{\rm cry}) \cdot \mathbf{E}^*_{ml}(2\theta_{\rm cry})|$.

According to both schemes, the diffraction profiles can be calculated from the electric fields inside or outside the crystal by using the dynamical theory of X-ray diffraction. Also both schemes give consistent results with the experiments as can be seen later in this paper. In addition, the first scheme could deliver diffraction profiles with the corresponding modes of wave propagation, and the second scheme provides the diffraction profiles without mode information.

3.3. Coordinate transformations

In the previous section, the crystal coordinate system (see Fig. 5*c*) is used in the algorithm for the X-ray crystal diffraction profile of the 2θ scan. In the crystal frame, the crystal surface parallel to the xy plane is defined as $2\theta_{\rm cry} = 0$. Because the crystal is placed at the centre of a diffractometer, the origin O of the laboratory coordinate system is located at the centre of the diffractometer. Fig. 5(*a*) shows the laboratory coordinate system and the experimental arrangement, where the x axis (denoted as $x_{\rm Lab}$) is along the incident-beam ($\mathbf{k}_O$) direction, and the $x_{\rm Lab}y_{\rm Lab}$ plane is in the equatorial plane. A detector is situated at the intersection of 2θ and β arcs, meaning the detector can be scanned vertically and horizontally. Fig. 5(*b*) shows two different reference frames: the

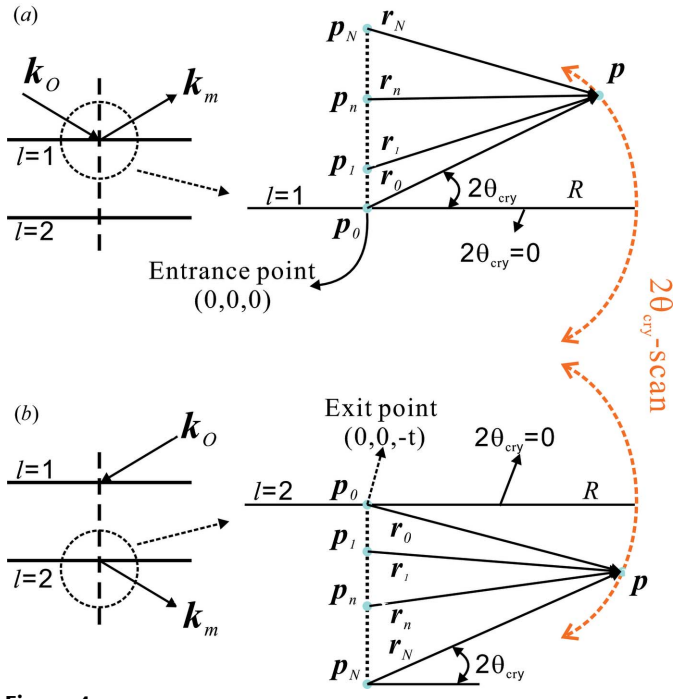

Figure 4
Schematic representation in the xz plane of the one-dimensional diffraction profile of the 2θ-scan algorithm with outside electric fields of the mth diffracted beam at (*a*) entrance surface ($l = 1$) for Bragg diffraction, and (*b*) exit surface ($l = 2$) for Laue diffraction. $\mathbf{k}_O$ and $\mathbf{k}_m$ stand for the wavevector of the incident beam and the wavevector of the mth diffracted beam outside the crystal.

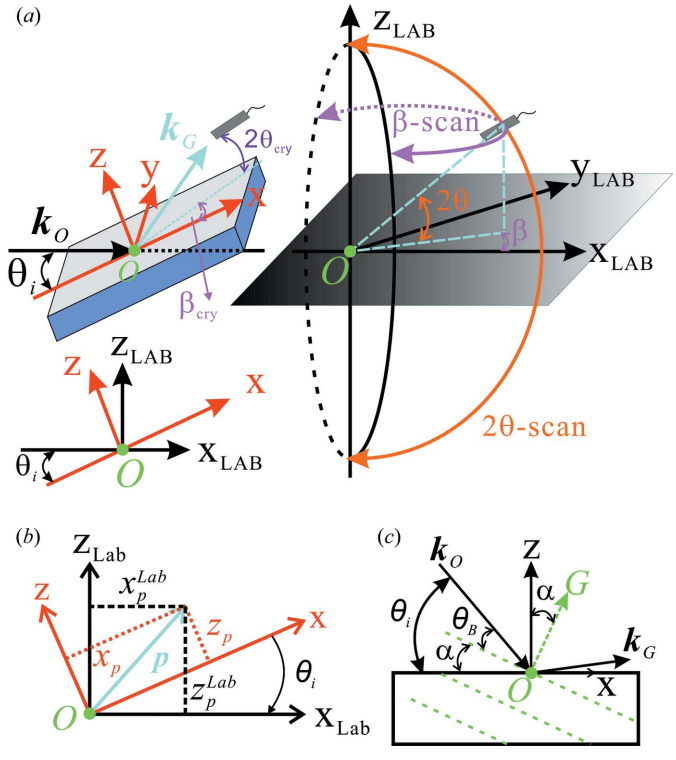

Figure 5
(*a*) Relationship between the laboratory coordinate system ($x_p^{\rm Lab}, y_p^{\rm Lab}, z_p^{\rm Lab}$) and the experimental setup (x, y, z). (*b*) The general transformation between two arbitrary frames. (*c*) The crystal coordinate system.

crystal coordinate system and the laboratory coordinate system. The position vector **p** in Fig. 5(*b*) can be expressed as $\mathbf{p} = (x_p, y_p, z_p)$ in the crystal system, or $\mathbf{p} = (x_p^{\rm Lab}, y_p^{\rm Lab}, z_p^{\rm Lab})$ in the laboratory coordinate system.

The relationship between these two coordinate systems can be expressed as follows:

$$\mathbf{p} = \begin{pmatrix} x_p^{\rm Lab} \\ y_p^{\rm Lab} \\ z_p^{\rm Lab} \end{pmatrix} = R_y(\theta_{\rm i}) \begin{pmatrix} x_p \\ y_p \\ z_p \end{pmatrix} = \begin{pmatrix} \cos\theta_{\rm i} & 0 & -\sin\theta_{\rm i} \\ 0 & 1 & 0 \\ \sin\theta_{\rm i} & 0 & \cos\theta_{\rm i} \end{pmatrix} \begin{pmatrix} x_p \\ y_p \\ z_p \end{pmatrix}. \quad (20)$$

$R_y(\theta_{\rm i})$ is a rotation matrix for a rotation of the system around the y axis by $\theta_{\rm i}$, where $\theta_{\rm i}$ is the incident angle. When the crystal system is rotated about the y axis by $\theta_{\rm i}$, the calculated diffracted profile of the $2\theta_{\rm cry}$ scan in the crystal coordinate system can be transformed into that in the laboratory coordinate system *via* the rotation matrix $R_y(\theta_{\rm i})$. In Fig. 5(*c*), the incident angle $\theta_{\rm i} = \theta_{\rm B} + \alpha$ is the angle between the crystal surface and the incident beam. $\theta_{\rm B}$ is the Bragg angle of the G-reflection and α is the angle between the atomic plane of the G-reflection and the crystal surface. α is expressed as $\alpha = \alpha_0 + \alpha_{\rm mis}$. $\alpha_0 = \cos^{-1}(\mathbf{OG} \times \hat{z}/|OG|)$ can be calculated from the z axis and reciprocal-lattice vector **OG**. $\alpha_{\rm mis}$ is the miscut between the crystal surface and the (hkl) atomic planes of the [hkl] wafer. If $\alpha_{\rm mis} = 0°$, for a symmetric Bragg diffraction α is 0°, and for a symmetric Laue diffraction α is 90°.

4. Case study

In this section an extremely asymmetric two-beam surface diffraction and a three-beam Bragg surface diffraction are discussed. As shown later, the calculated results not only provide the diffraction profiles of the 2θ scan but also reveal the relationship between the excited modes and the diffracted beams. For an extremely asymmetric two-beam surface diffraction, three beams are observed. One is the incident beam, one is the surface diffracted beam and the other one is the specular surface reflected beam. It shows the one-to-one correspondence of the excited modes to the diffracted beams, which occur at different 2θ. For three-beam surface diffraction, four beams are observed. One is the incident beam, two are diffracted beams, and the last one is the specular surface reflected beam. It shows the diffraction profiles with the corresponding modes of wave propagation.

Fig. 6 shows a schematic of the 2θ-scan experimental setup. The experiment was performed at the 25-pole wiggler beamline 17B1 at the National Synchrotron Radiation Research Center (NSRRC), Taiwan. The incident beam defined by an Si(111) double-crystal monochromator was σ-polarized with the beam size about 0.5 × 0.6 mm (V × H). The acceptance angle and energy resolution are 4(H) × 0.3(V) mrad and 2×10^{-4}, respectively. The distances from the beam source to the monochromator and to the sample crystal are about 23.9 and 42 m, respectively (see http://www.nsrrc.org.tw/). The sample crystal was placed at the centre of an eight-circle diffractometer at beamline 17B1. The 2θ scan is performed when the sample crystal is at a fixed $\theta_{\rm i}$ and a scintillation detector is placed on the detector arm which can be rotated along 2θ and β circles, as shown in Fig. 5(*a*). The detector is moving during the measurement. The diffracted beam was monitored by a scintillation detector placed 100 cm away from the centre of the diffractometer. In consideration of the beam divergence in the vertical direction, all the calculated diffraction profiles were convoluted with a Gaussian function, whose FWHM is the same as that of the incident beam.

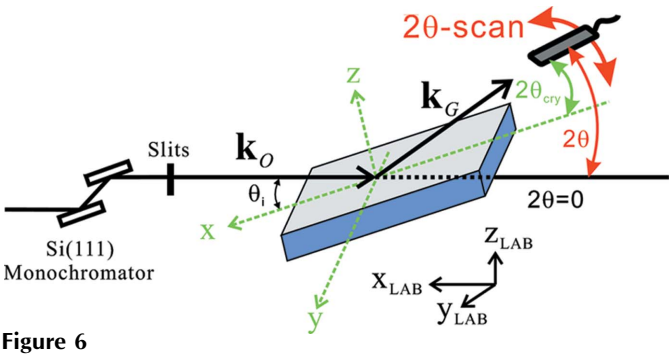

Figure 6
Schematic of the 2θ-scan experimental setup.

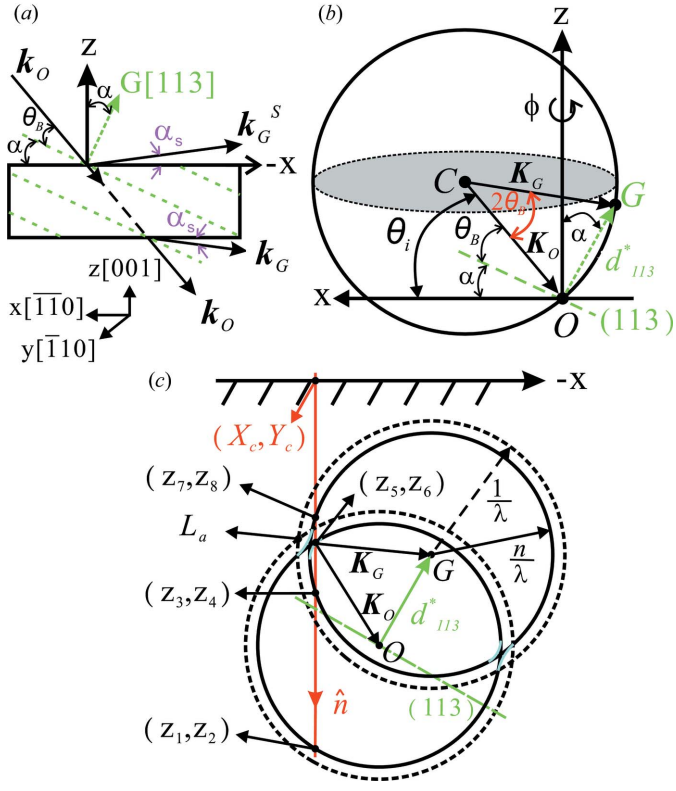

Figure 7
Schematic of extremely asymmetric two-beam (000)(113) grazing-emergence Laue diffraction of silicon at energy 8.9 keV in (*a*) real space, (*b*) reciprocal space and (*c*) the dispersion surface.

4.1. Extremely asymmetrical two-beam surface diffraction

For an extremely asymmetric two-beam surface diffraction, the angle α_s between the diffracted beam $\mathbf{k}_G$ and the crystal surface (Fig. 7*a*) is smaller than the critical angle of the total reflection, and specular reflection occurs. This is also called grazing emergence (Authier, 2005). It is a two-beam diffraction case, but three beams are observed. Fig. 7(*a*) shows the diffraction geometry of the grazing-emergence Laue diffraction of Si(000)(113) of a [001] silicon crystal. The thickness of this crystal is 650 µm. The Cartesian coordinate frame is chosen such that the *x*, *y* and *z* axes are parallel to $[\bar{1}10]$, $[1\bar{1}0]$, and [001], respectively. The dashed lines represent the atomic plane (113). $\mathbf{k}_O$, $\mathbf{k}_G$ and $\mathbf{k}_G^S$ are the incident, surface diffracted and specularly reflected wavevectors outside the crystal, respectively. In Fig. 7(*b*), the reciprocal-lattice points *O* and *G* are on the surface of the Ewald sphere. Point *C* is the centre of the Ewald sphere. $\mathbf{K}_O$ and $\mathbf{K}_G$ are the incident and diffracted wavevectors inside the crystal, respectively. The length of the reciprocal-lattice vector **OG** is d^*_{113}.

The Laue diffracted beam $\mathbf{k}_G$ transmits through the crystal and the specular reflected beam $\mathbf{k}_G^S$ propagates into the air from the entrance surface. In this case, the photon energy is *E* = 8.9 keV (λ = 1.393 Å) and the Bragg angle θ_B of (113) is 25.174°. The miscut between the crystal surface and the (001) atomic planes of the [001] silicon wafer was determined by using the specular reflection of the entrance surface and the (004) diffraction for the two in-plane directions [110] and $[1\bar{1}0]$. The smaller miscut α_{mis} is about 0.113° along [110]. The angle between the atomic plane (113) and crystal surface is $\alpha = \cos^{-1}[3/(11)^{1/2}] + \alpha_{mis} = 25.3525°$. The incident angle θ_i in Fig. 7(*b*) can be calculated as $\theta_i = \theta_B + \alpha = 50.5265°$.

Fig. 7(*c*) shows the intersection of the dispersion surface (solid curves) with the plane of incidence for the extremely asymmetric two-beam Si(000)(113) surface diffraction at *E* = 8.9 keV. The dashed and solid spheres centred at *O* and *G* represent the Ewald spheres outside and inside the crystal, respectively. The radii of dashed and solid spheres are $1/\lambda$ and n/λ, respectively, where *n* is the refractive index of the Si crystal at *E* = 8.9 keV. The dashed and solid spheres intersect at L_a (Laue point) and L_o (Lorentz point), respectively. The Lorentz point L_o is approximately located at point *C* in Fig. 7(*b*). Similar to symmetrical two-beam Laue diffraction (Chang, 2004), the excitation of the dispersion surface generates eight possible modes of wave propagation, including four σ-polarized modes, z_2, z_4, z_6, z_8, and four π-polarized modes, z_1, z_3, z_5, z_7. Modes 1 and 2 can be neglected because these two modes are far from the Laue point L_a. The Laue point is located at $k\zeta_r(j) = 0$ and $\Delta\theta = 0$ (see Fig. 8*a*). Moreover, the peak of the calculated rocking curve is located at

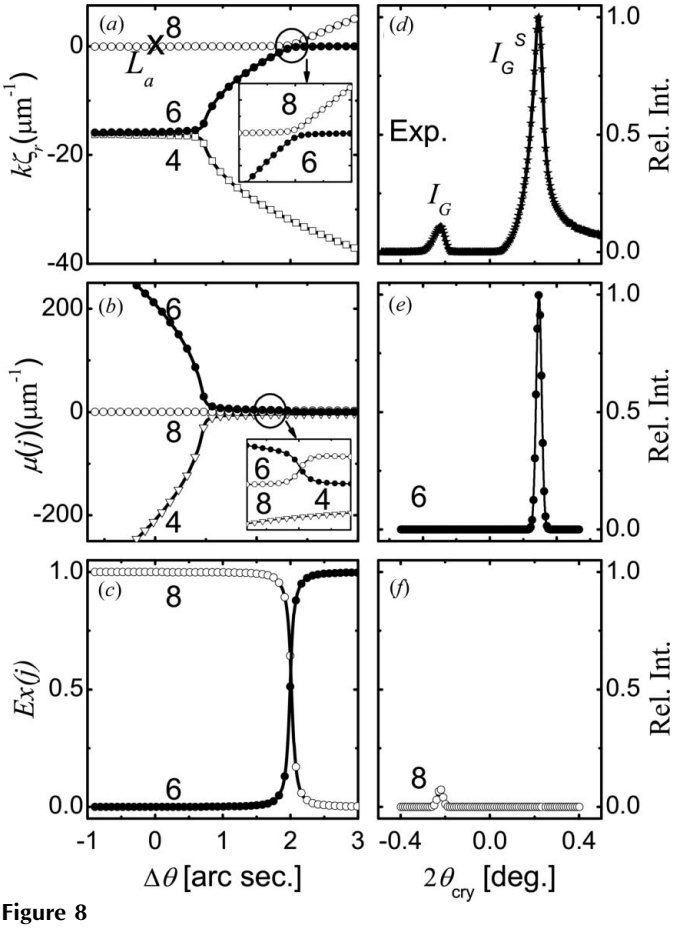

Figure 8
Dynamical calculations: (*a*) dispersion surface, (*b*) linear absorption coefficients, (*c*) excitation of mode, (*d*) measured integrated intensity, and calculated intensities of (*e*) mode 6 and (*f*) mode 8 for an extremely asymmetric (113) grazing-emergence Laue diffraction of silicon at *E* = 8.9 keV.

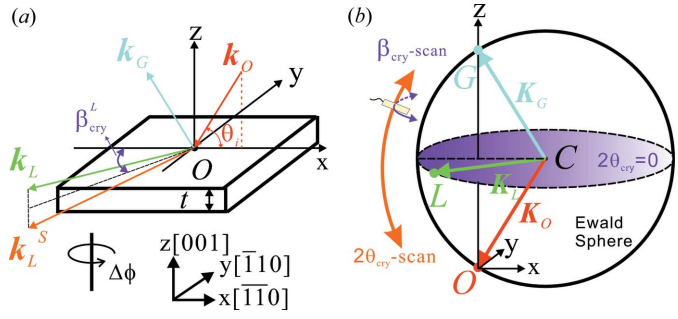

Figure 9
Schematic representation of symmetric three-beam (*O*, *G*, *L*) Bragg surface diffraction geometry in (*a*) real space, (*b*) reciprocal space.

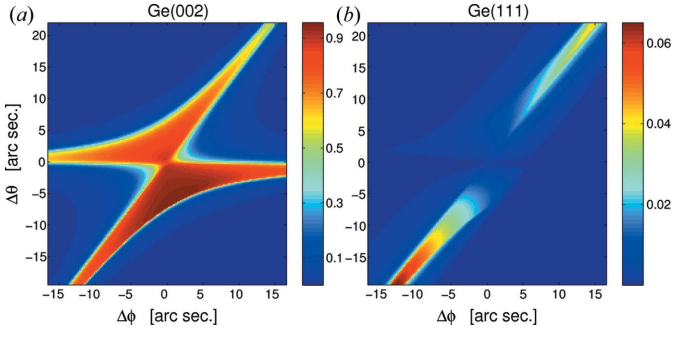

Figure 10
Calculated intensity distribution of (*a*) *G*(002) and (*b*) *L*(111) for the three-beam Ge(000)(002)(111) diffraction at *E* = 10 keV with a σ-polarized incident radiation.

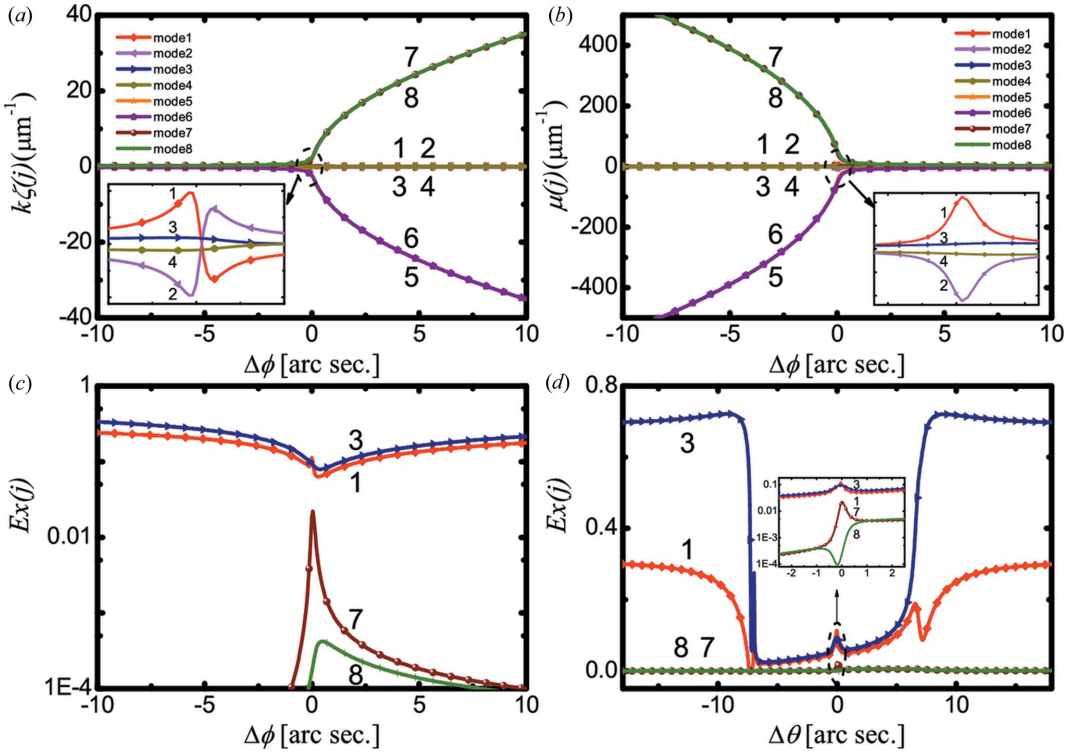

Figure 11
(*a*) Calculated dispersion surface and (*b*) calculated linear absorption coefficients for the three-beam Ge(000)(002)(111) diffraction at $E = 10$ keV with a σ-polarized incident radiation. Calculated excitation of modes *versus* (*c*) azimuth angle ($\Delta\varphi$) and (*d*) incident angle ($\Delta\theta$).

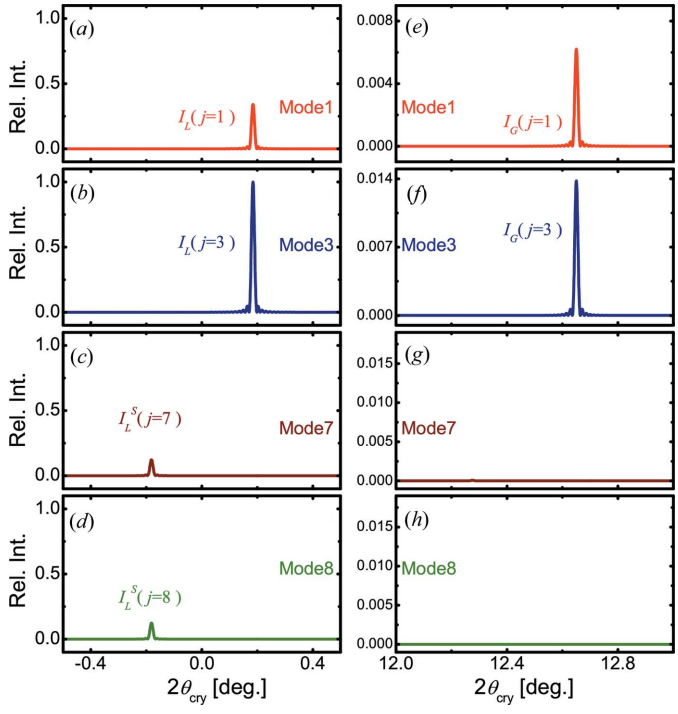

Figure 12
The calculated diffraction profiles ($2\theta_{cry}$ scan): (*a*)–(*d*) modes 1, 3, 7 and 8 for (111) and (*e*)–(*h*) modes 1, 3, 7 and 8 for (002) in the three-beam Ge(000)(002)(111) case at $E = 10$ keV in the crystal coordinate frame. The electric fields *inside* the crystal obtained from the dynamical theory are used.

$\Delta\theta = 2.017''$ (not shown). Hence, the incident angle for the calculated diffraction profile (2θ scan) is about 50.52706°.

Figs. 8(*a*), 8(*b*) and 8(*c*) are the calculated dispersion surface [$k\zeta_r(j)$], linear absorption coefficient [$\mu(j)$] and excitation of mode [$E_x(j)$] of the extremely asymmetric two-beam Si(000)(113) surface diffraction at $E = 8.9$ keV *versus* $\Delta\theta$ (Stetsko & Chang, 1997; Authier, 2005; Chang, 2004), respectively. $\Delta\theta$ is the angular deviation from the incident angle θ_i. Because of the σ-polarized incident beam, only the dispersion curves of modes 4, 6 and 8 are shown in Fig. 8(*a*). In Fig. 8(*b*), according to the conservation of energy, mode 4 with negative absorption coefficient is discarded. Hence, only modes 6 and 8 are active and whose excitations of mode are plotted in Fig. 8(*c*). As can be seen, the excitations of these two modes behave in an opposite manner to each other, mode 6 increasing and mode 8 decreasing, and both have the same excitation (50%) at $\Delta\theta = 2.017''$.

Figs. 8(*d*), 8(*e*) and 8(*f*) are the measured and calculated diffraction profiles for Si(113) grazing-emergence Laue diffraction in the crystal coordinate. $2\theta_{cry}$ is the angular deviation with respect to the position of the crystal surface, *i.e.* $2\theta_{cry} = 0°$. For the dynamical calculation, the electric fields inside the crystal are adopted. The depth p_N and the distance between adjacent oscillators Δp are chosen as 1 μm and 1 Å, respectively. Moreover, the *Pendellösung* distance calculated is $L = 1.2$ μm for this case.

In Fig. 8(*d*), the (113) Laue diffracted beam with the intensity I_G and the specularly reflected beam with the intensity I_G^S are observed. Comparison of the experimental

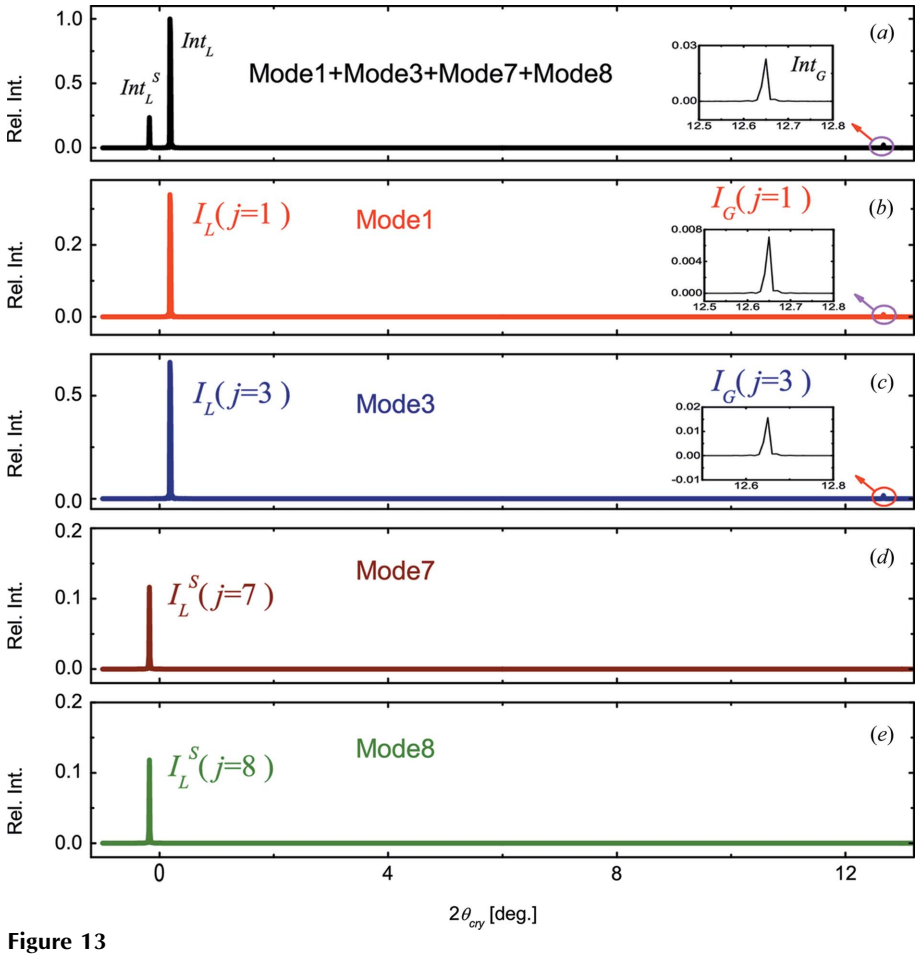

Figure 13
The connection between the calculated diffraction profiles and the excitation of modes for three-beam Ge(000)(002)(111) at E = 10 keV using the electric fields *inside* the crystal obtained from the dynamical theory.

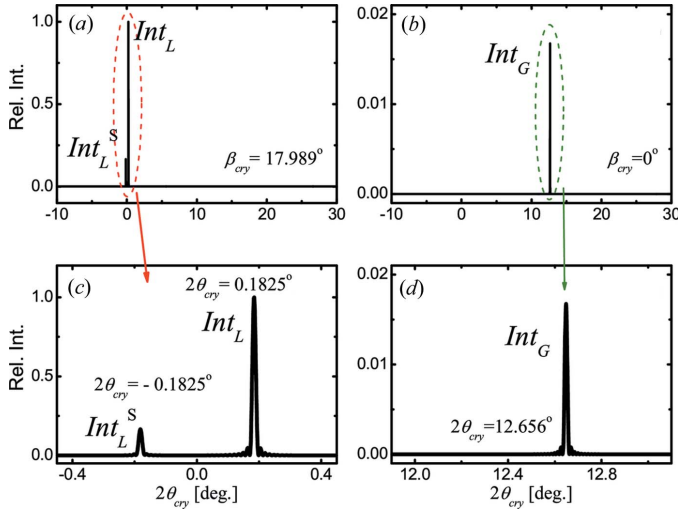

Figure 14
The calculated diffraction profile ($2\theta_{cry}$ scan) of (*a*) *L* beam (111) and (*b*) *G* beam (002) for three-beam Ge(000)(002)(111) at E = 10 keV in the crystal coordinate frame using the electric fields *outside* the crystal obtained from the dynamical theory. (*c*) and (*d*) are the details of (*a*) and (*b*), respectively.

data (Fig. 8*d*) with the calculated intensities for modes 6 and 8 (Figs. 8*e* and 8*f*) shows that I_G^S and I_G result from the excitation of modes 6 and 8, respectively. The connection between the diffraction profiles of 2θ scans and the excited modes is evident in this case.

4.2. Three-beam Bragg surface diffraction

The three-beam Bragg surface diffraction, Ge(000)(002)(111), was investigated. The primary reflection $G(002)$ and the secondary reflection $L(111)$ of a three-beam (O, G, L) diffraction involves a symmetric Bragg reflected beam ($\mathbf{K}_G$), a surface reflected beam ($\mathbf{K}_L$) and a specular surface reflected beam ($\mathbf{K}_L^S$). Fig. 9 shows the diffraction geometry in (*a*) real space and (*b*) reciprocal space. The Cartesian coordinate frame is chosen such that the x, y and z axes are parallel to $[\bar{1}\bar{1}0]$, $[1\bar{1}0]$ and [001], respectively. Both the Bragg diffracted beam $\mathbf{K}_G$ and the surface reflected beam $\mathbf{K}_L$ propagate into the air from the entrance surface, and the specularly reflected beam $\mathbf{K}_L^S$ transmits through the crystal. In this case, the photon energy is E = 10 keV (λ = 1.2398 Å) and the Bragg angle θ_B of (002) is 12.6534°.

Fig. 10 shows the calculated intensity distributions of the primary $G(002)$ reflection and the secondary $L(111)$ reflection for the three-beam (000)(002)(111) diffraction of Ge and E = 10 keV with a σ-polarized incident radiation. The Lorentz point (L_o) is located at $\Delta\theta = 0$ and $\Delta\varphi = 0$, *i.e.* the angular position of the calculated rocking-curve peak. Hence, the incident angle for the calculated diffraction profile (2θ scan) is about 12.6559°.

There are 12 possible modes of propagation in this case. Modes 1 to 4 are associated with the symmetric (002) Bragg reflection and modes 5 to 8 are related to the (111) surface reflection. Modes 9 to 12 can be neglected because these four modes are very far from the Lorentz point (not shown in Fig. 11). The calculated dispersion surface and linear absorption coefficients for modes 1 to 8 are shown in Figs. 11(*a*) and 12(*b*), respectively. According to the conservation of energy, modes 2, 4, 5 and 6 with negative absorption coefficient are discarded. Hence, only modes 1, 3, 7 and 8 are active.

In this case, the depth p_N and the distance between adjacent oscillators Δp are chosen as 500 nm and 1 Å, respectively. The step size of $\Delta 2\theta_{cry}$ is 1 Å. Fig. 12 shows the calculated $2\theta_{cry}$ scan of the diffraction profile for three-beam Ge(000)(002)(111) diffraction at E = 10 keV in the *crystal*

coordinate frame using the electric field *inside* the crystal obtained from the dynamical theory.

Figs. 12(*a*) to 12(*d*) provide the calculated diffraction profiles of the surface diffracted beam (I_L) and specularly reflected beam (I_L^S) for modes 1, 3, 7 and 8. For the Bragg diffracted beam (I_G), Figs. 12(*e*) to 12(*h*) are the calculated diffraction profiles for these four active modes. The intensities of the remaining eight modes are null. According to the calculated results, the (002) Bragg diffracted beam with the intensity Int_G results from modes 1 and 3. The (111) surface diffracted beam with the intensity Int_L results from modes 1 and 3. The (111) specularly reflected beam with the intensity Int_L^S originates from modes 7 and 8.

Fig. 13 shows the relation between calculated diffraction profiles and the excitation of modes for three-beam Ge(000)(002)(111) diffraction at $E = 10$ keV using the electric fields *inside* the crystal obtained from the dynamical theory. Modes 1 and 3 contribute to the Bragg diffracted beam $\mathbf{K}_G$ and the surface reflected beam $\mathbf{K}_L$. Modes 7 and 8 contribute to the specularly reflected beam $\mathbf{K}_L^S$. Fig. 14 shows the calculated $2\theta_{\mathrm{cry}}$ scan of the diffraction profile for three-beam Ge(000)(002)(111) at $E = 10$ keV in the crystal coordinate frame using the electric fields *outside* the crystal obtained from the dynamical theory. Both schemes give the same diffracted profiles.

5. Conclusion

In conclusion, we have proposed in this paper an algorithm to calculate the X-ray crystal diffraction profile of the 2θ scan based on the dynamical theory of X-ray diffraction. A diffraction pattern can be calculated by using the electric fields inside or outside a crystal. Both give the 2θ-scan profiles in good agreement with the experimental observation. Comparing the experimental and calculated results obtained with the electric fields inside the crystal, the connection between the diffraction profile of the 2θ scan and the excitation of mode can be obtained. Moreover, for extremely asymmetric diffraction, the diffraction profile of the 2θ scan due to different modes can be separately detected at different 2θ angles. The reason is that the excitation of the dispersion surface depends on the crystal entrance surface relative to the atomic planes participating in the diffraction. Usually for wide-angle diffraction, it is not possible to tell which measured intensities (2θ scan) correlate with which individual modes, unless the diffraction is extremely asymmetric. For extremely asymmetric grazing-emergence Laue diffraction, the portion of the excited dispersion surface is asymmetric and the most intense excitation occurs near the region where mode 6 and mode 8 are nearly crossed over (Fig. 8*a*). This means that two diffraction peaks of modes 6 and 8 appear at different 2θ angles (Figs. 8*e* and 8*f*). For three-beam Bragg surface diffraction, the most intense excitation occurs near the L_o point (Fig. 11). This means that modes 1 and 3 contribute to the Bragg diffracted beam $\mathbf{K}_G$ and the surface reflected beam $\mathbf{K}_L$, while modes 7 and 8 contribute to the specularly reflected beam $\mathbf{K}_L^S$. This algorithm is not only suitable for a single crystal but also for nano-structures on a crystal substrate (Chen *et al.*, 2014).

Furthermore, this algorithm using the diffracted electric fields with proper boundary conditions should be quite general and suitable for calculations in many diffraction geometries, including, for example, extremely asymmetric diffraction and back diffraction.

We are indebted to H.-Y. Lee for his excellent experimental help at BL 17B1, NSRRC. We also thank the Ministry of Education and National Science Council for financial support.

References

Als-Nielsen, J. & McMorrow, D. (2011). *Elements of Modern X-ray Physics.* New York: Wiley.
Authier, A. (2005). *Dynamical Theory of X-ray Diffraction*, 3rd ed. Oxford University Press.
Chang, S.-L. (2004). *X-ray Multiple-Wave Diffraction: Theory and Application.* Berlin: Springer-Verlag.
Chen, H.-Y., Chu, P.-T. & Chang, S.-L. (2014). *J. Appl. Cryst.* **47**, 285–290.
Chiu, M.-S., Stetsko, Yu. P. & Chang, S.-L. (2008). *Acta Cryst.* A**64**, 394–403.
Darwin, C. G. (1914). *Philos. Mag.* **27**, 675–690.
Ewald, P. P. (1916). *Ann. Phys. (Leipzig)*, **49**, 1–38.
Hecht, E. (2002). *Optics.* San Francisco: Addison Wesley.
Kato, N. (1960). *Acta Cryst.* **13**, 349–356.
Kohn, V. G., Gorobtsov, O. Y. & Vartanyants, I. A. (2013). *J. Synchrotron Rad.* **20**, 258–265.
Kohn, V. G., Snigireva, I. & Snigirev, A. (2000). *Phys. Status Solidi B*, **222**, 407–423.
Laue, M. von (1931). *Ergeb. Exakten Naturwiss.* **10**, 133–158.
Saleh, B. E. A. & Teich, M. C. (2007). *Fundamentals of Photonics.* New York: Wiley-Interscience.
Stetsko, Yu. P. & Chang, S.-L. (1997). *Acta Cryst.* A**53**, 28–34.